Synthetic State of Charge Estimation for Lithium-ion Batteries Based on Long Short-Term Memory Network Modeling and Adaptive H-Infinity Filter

Zheng Chen[1, 2], Hongqian Zhao[1], Xing Shu[1], Yuanjian Zhang[3], Jiangwei Shen[1**] and Yonggang Liu[4*]
[1]Faculty of Transportation Engineering, Kunming University of Science and Technology, Kunming, 650500, China
[2]School of Engineering and Materials Science, Queen Mary University of London, London, E1 4NS, United Kingdom
[3]School of Mechanical and Aerospace Engineering, Queen's University of Belfast, BT9 5AG, Northern Ireland
[4]State Key Laboratory of Mechanical Transmissions & School of Automotive Engineering, Chongqing University, Chongqing, 400044, China
Email: chen@kust.edu.cn, zhaohongqian@stu.kust.edu.cn, shuxing92@kust.edu.cn, y.zhang@qub.ac.uk, shenjiangwei6@163.com, andylyg@umich.edu
Corresponding author: Yonggang Liu (andylyg@umich.edu) and Jiangwei Shen (shenjiangwei6@163.com)

Abstract: Accurate state of charge estimation is essential to improve operation safety and service life of lithium-ion batteries. This paper proposes a synthetic state of charge estimation method for lithium-ion batteries based on long short-term memory network modeling and adaptive H-infinity filter. Firstly, the long short-term memory network is exploited to roughly estimate state of charge with the input of voltage, current, operating temperature and state of health. Then, to mitigate the output fluctuation and improve the estimation robustness of long short-term memory network, the adaptive H-infinity filter is employed to flatten the estimation results and further improve the estimation accuracy. A main advantage of the proposed synthetic method lies in that precise battery modeling and burdensome model parameter identification tasks that are imperative in traditional observers or filters can be omitted, thus improving the application efficiency of the proposed algorithm. The proposed method is verified effective on two types of lithium-ion batteries under dynamic working scenarios including the varying temperature and aged conditions. The experimental results highlight that the estimation error of state of charge can be restricted within 2.1% in wide temperature range and different aging states, manifesting its high-precision estimation capacity and strong robustness.

Key Words: Lithium-ion batteries, state of charge, long short-term memory network, adaptive H-infinity filter.

I. INTRODUCTION

To alleviate energy crisis, greenhouse gas emission as well as environmental pollution, massive efforts have been made through emergent enabling technologies, such as transportation electrification [1]. Electric vehicles

(EVs), as one of the representative solutions, have attracted substantial attention due to the prosperous development of energy storage technologies [2]. Currently, lithium-ion batteries (LIBs), as a mainstream energy storage media, have been widely deployed in EVs thanks to their high energy/power density, wide operating temperature capacity and long lifespan [3]. Consequently, high-efficiency management/control of LIBs, usually attained by the so-called battery management system (BMS), is of great significance to improve operation safety of batteries, extend their lifespan, and furthermore optimize energy economy of EVs. Among all the management tasks, one critical job is to estimate the battery state of charge (SOC), which represents the ratio of the remaining capacity over the nominal capacity [4]. The estimation accuracy of SOC can directly affect other functions of BMS, including state of health (SOH), thermal management, balance activities and charge control [5]. In addition, accurate SOC estimation can supply important reference for operating efficiency promotion of vehicle powertrain [6]. As SOC cannot be directly measured from external measures, but can only be estimated indirectly according to the hidden relationship between SOC and physical quantities such as voltage, current and temperature [7]. Actually, SOC can be easily influenced by different factors like aging, ambient temperature and charge/discharge efficiency, leading to certain difficulties for high-quality estimation [8].

Currently, a large number of advanced methods have emerged for accurate SOC estimation, such as Ampere hour (Ah) integration method [9], open circuit voltage (OCV) based methods [10], electrochemical impedance methods [11], model based filtering methods [12] and data-driven methods [13]. The Ah integration method is simple and easy to implement. Nonetheless, it highly depends on the precise knowledge of initial SOC and rated capacity as well as the accuracy of current sensor/transducer [14], and the accumulation of sensor error may raise aggravated difference from actual values [15]. The OCV based method is widely accepted as an offline SOC estimation strategy, and the basic principle is to establish a OCV-SOC mapping table according to the nonlinear relationship between SOC and OCV [16]. However, accurate OCV value can be obtained only after shelving the battery for quite long time [17], making it difficult to implement in practice [18]. The electrochemical impedance based method can estimate SOC via measuring the internal impedance of batteries; which, however, is highly affected by the external environment, and is difficult to measure online but more suitable for offline calibration [19]. Model based filtering methods usually establish observation models to bridge the implicit SOC with the measured current, voltage and other related variables; and on this basis, the SOC estimation is conducted by

different filter/observer algorithms [20], involving Kalman filter (KF), extended KF (EKF) [21], unscented particle filter (UPF) [22], H-infinity filter (HIF) [23], adaptive unscented KF (AUKF) [24], etc. Among them, HIF can circumscribe the noise interference within a limited H-infinity norm of the state estimation error, thus efficiently mitigating the opposite influence due to the model uncertainty and improving the robustness of estimation. However, in existing solutions to SOC estimation, traditional HIF and adaptive HIF (AHIF) are mainly based on equivalent circuit model (ECM). For instance, Ref. [25] exploits a multi-scale dual HIF to estimate battery SOC and capacity simultaneously based on the ECM. To attain the SOC estimation, an indispensable task is that the parameters of ECM need to be identified in advance by various algorithms such as genetic algorithm (GA) and least square methods. However, the influences of temperature, current, voltage and degradation on SOC are difficult to be incorporated in a fixed ECM, and imprecise parameters will certainly lead to unreliable modeling performance and also be unfavorable for SOC estimation [26]. To cope with it, data-driven methods began to attract substantial attention, as they do not need the detailed knowledge in terms of complicated electrochemical reactions inside of battery, but merely learn the latent nonlinear relationship among SOC and external measures [27]. Typical data-driven algorithms include support vector machine (SVM) [28] and neural network (NN) [29]. In [30], radial basis function (RBF) NN applies a hidden layer with RBF units to analyze the relationships between the input sequence (terminal voltage, current and actual capacity) and target values (SOC). According to the Ah integration method, one can know that the SOC estimation is essentially a time series forecasting problem; whereas the traditional data-driven algorithms assume that all the inputs and outputs are independent of time sequence and cannot effectively estimate SOC according to the historical information; therefore, the estimation accuracy of these methods cannot be guaranteed all the time, especially under the varying temperature and aged conditions. With the development of NN, recurrent NN (RNN) has become one of the most promising solutions for SOC estimation due to its strong capacity of dealing with historical operation data and time series information. In [31], battery's voltage, current and ambient temperature variation are imported to estimate battery's SOC based on the trained RNN model, and the results highlight that RNN features better SOC estimation capability than classical multilayer perception models. However, conventional RNNs usually face with gradient explosion and gradient vanishing during back propagation, and thus they usually cannot capture long-term dependence. To tackle this drawback, Ref. [32] proposes long short-term memory (LSTM) network evolved from RNN to capture the long-term

dependencies through its specific gate structure. Moreover, compared with RNN, LSTM network shows higher nonlinear modeling capability and more accurate prediction performance in processing time sequential data, such as SOC estimation. In [33], the LSTM is successfully applied to raise the high-quality estimation of SOC. Nevertheless, the LSTM based method shows the following two shortcomings. Firstly, the selection of hyper-parameters highly depends on experience and iterative optimization, making it quite challenging to find the optimal values. Secondly, the LSTM method cannot mitigate the influence of measurement noise on SOC estimation due to its weak robustness, resulting in obvious fluctuation of estimation results once the non-negligible noises emerge. Actually, both drawbacks also exist in conventional NN based methods. To overcome them, fusion algorithms incorporating NN and filtering methods are developed for more accurate and reliable SOC estimation [34]. Ref. [35] integrates the feedforward NN and UKF to estimate SOC with the desired estimation accuracy at different temperatures. Nonetheless, the generalization ability on other batteries still needs to be investigated and validated.

In light of these concerns, a novel synthetic SOC estimation method is presented based on LSTM and AHIF. Firstly, the LSTM network is designed to mimic the sophisticated dynamic characteristics of two types of lithium-ion batteries and predict the SOC on account of the acquired voltage, current, temperature and SOH variations. Then, the AHIF, which is robust to parameter uncertainty and modeling error, is employed to smooth the SOC obtained through LSTM and improve the robustness of LSTM network output [3]. Compared with the traditional model based filtering methods and the LSTM with the conventional HIF (LSTM-HIF for short) method, the proposed method exhibits better estimation accuracy and faster convergence speed when encountered with incorrect initial SOC values. Additionally, the validation results highlight that the proposed method does not need to build a precise battery model or determine the model parameters with effort, and thus the time-consuming and cumbersome model identification process can be effectively alleviated. The main contributions of this paper can be summarized into the following two aspects:

1) A synthetic SOC estimation algorithm is developed based on the LSTM and AHIF. Compared with other fusion methods, the proposed method improves the estimation accuracy and robustness while maintaining the reasonable simplicity. In addition, the model features strong generalization and universality for two different types of batteries, of which the positive electrode materials are respectively lithium iron phosphate (LFP) and lithium nickel cobalt manganese (NCM).

2) The proposed method can estimate SOC with high precision under wide temperature range and different aging state. Moreover, the short estimation time of each step (less than 1 ms) is verified suitable for real-time application.

The remainder of this paper is organized as follows: Section II introduces the LSTM network used for SOC estimation. Section III details the AHIF and the synthetic estimation process based on LSTM network and AHIF. Section IV presents the results and discussions of the proposed method. Finally, the brief conclusions are summarized in Section V.

II. LSTM Network Based SOC Estimation

A. Introduction of LSTM Network

RNN is developed based on the Hopfield NN [36], and has been widely applied in various tasks such as natural language processing, time series forecasting and system modeling [37]. The key feature of RNN is that the nodes of hidden layers are connected with each other. By this manner, the temporal correlation of the input signal can be learned, and the influence of historical sequence information on current output can be fully considered. In theory, RNN can model time series data with any length; whereas in practice, it is difficult to capture long-term temporal dependency, as RNN can easily face with gradient vanishing and gradient explosion in the process of adjusting the node/unit parameters via the back propagation through time (BPTT) algorithm, especially when the model depth increases.

LSTM network is an extended format of RNN. Compared with typical RNNs, LSTM network adds different gates to control the flow of information. Fig. 1 (a) shows the structure of LSTM unit, which includes a forget gate, an input gate, an output gate and different input-output connections controlled by these gates. The three gate units constitute the core part of the LSTM network, and ensure that the LSTM unit can store and update information. The forgetting gate is responsible for deleting the state information in the LSTM unit; the input gate selects the useful input information and transmits it to the memory unit; and the output gate controls how much information calculated in the memory unit will be delivered to the output.

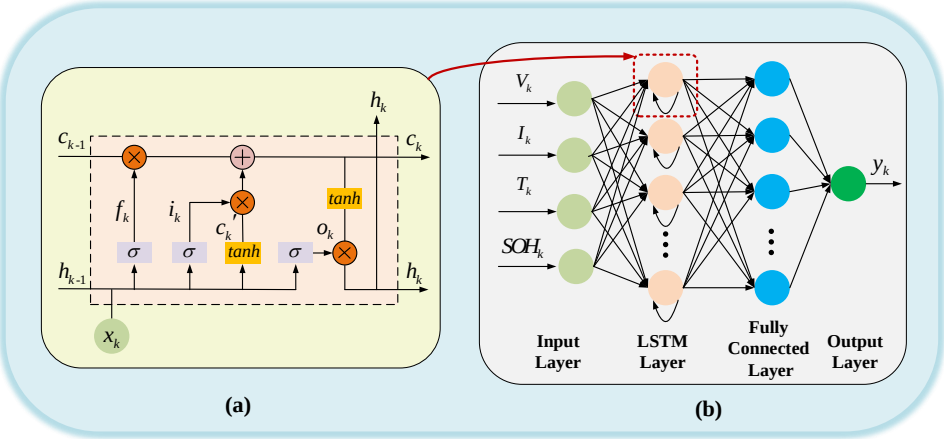

Fig. 1. LSTM topology. (a) Structure of LSTM unit; (b) Structure of LSTM network.

The calculation process at time k for the forward pass of in LSTM unit can be detailed, as:

$$f_k = \sigma(w_f \cdot [h_{k-1}, x_k] + b_f) \tag{1}$$

$$c'_k = tanh(w_c \cdot [h_{k-1}, x_k] + b_c) \tag{2}$$

$$i_k = \sigma(w_i \cdot [h_{k-1}, x_k] + b_i) \tag{3}$$

$$c_k = f_k \otimes c_{k-1} + i_k \otimes c'_k \tag{4}$$

$$o_k = \sigma(w_o \cdot [h_{k-1}, x_k] + b_o) \tag{5}$$

$$h_k = o_k \otimes tanh(c_k) \tag{6}$$

where x_k and h_k denote the input and output of the LSTM unit at time k; f_k, i_k, c_k and o_k represent the forget gate, input gate, memory cell and output gate, respectively; w and b indicate the weight matrix and bias parameters to be learned during the training process; c'_k is the intermediate variable; $\sigma(\bullet)$ and tanh($\bullet$) are the sigmoid and hyperbolic tangent activation functions, as:

$$\sigma(x) = \frac{1}{1+e^{-x}} \tag{7}$$

$$tanh(x) = \frac{e^{x} - e^{-x}}{e^{x} + e^{-x}} \tag{8}$$

The output value of the sigmoid activation function is restricted within 0 and 1, and the output value of the hyperbolic tangent activation function is located between -1 and 1. Therefore, the inputs should be normalized to [-1, 1], which can improve the training efficiency and robustness of the LSTM network, as:

$$x_{norm} = \frac{2(x - x_{min})}{x_{max} - x_{min}} - 1 \tag{9}$$

where x_{min} and x_{max} denote the minimum and maximum values in the input vector x.

B. LSTM Network for SOC Estimation

Fig. 1 (b) shows the SOC estimation model with one LSTM hidden layer, wherein the influence of dynamic operating conditions, temperature and capacity degradation on SOC estimation are fully taken into consideration. The model input includes voltage, current, temperature and SOH; that is, $x_k = [V_k \ I_k \ T_k \ SOH_k]$. In addition, a full connection layer and an output layer are connected behind the hidden layer. As one of the most important components in NN, activation function plays a critical role in learning process [38], and mainly accounts for mapping the relationship between the input and output of neurons. The activation function can be divided into two types: linear activation function and nonlinear activation function. Compared with nonlinear activation function, linear activation function features the advantages of simpler structure and faster learning speed [39]. Since this study mainly focuses on the regression problem, and the full connection layer and the output layer do not need to deal with complex activation functions for nonlinear processing, the linear activation function is chosen as the activation function. Then, the estimated SOC_k can be attained, as:

$$\begin{cases} g_k = f(V_g h_k + b_g) \\ SOC_k = f(V_y g_k + b_y) \end{cases} \tag{10}$$

where g_k represents the output of the full connection layer, $f(\bullet)$ refers to the linear activation function, V_{g} and b_g respectively denote the weight matrix and bias parameters of the fully connected layer, V_y and b_y mean the weight matrix and bias parameters of the output layer. During the training process, the mean square error (MSE) is considered as the loss function of LSTM:

$$MSE = \frac{1}{K}\sum_{k=1}^{K}(SOC_k - SOC_k^*)^2 \tag{11}$$

In addition, three different error functions, including root mean square error (RMSE), maximum absolute error (MAX) and mean absolute error (MAE), are hired to evaluate the SOC estimation performance of LSTM network, as:

$$\begin{cases} RMSE = \sqrt{\frac{1}{K}\sum_{k=1}^{K}(SOC_k - SOC_k^*)^2} \\ MAX = max\left(\left|SOC_k - SOC_k^*\right|\right) \\ MAE = \frac{1}{K}\sum_{k=1}^{K}\left|SOC_k - SOC_k^*\right| \end{cases} \tag{12}$$

where K is the length of the time series, SOC_k^* represent the reference SOC value at time step k. In this paper, the adaptive momentum estimation (Adam) algorithm is applied to optimize the gradient, thanks to the advantage combination of AdaGrad and RMSProp algorithm and the capability of adaptive learning rate calculation for different parameters with less storage requirements [40]. In addition, overfitting during the training process often emerges [41]. n order to avoid its occurrence and enhance the generalization ability of the model, the dropout technique is leveraged between the LSTM hidden layer and the fully connected layer [42]. The main manner is to randomly set the output of some neurons to zero during training. While during the testing process, the dropout technology is not executed, and thus it will not affect the output of neurons [43]. The optimal dropout rate in this study is set as 0.2 through iterative optimization.

In the next step, the proposed AHIF algorithm will be addressed and applied for SOC estimation.

III. Adaptive H-Infinity Filtering Application for SOC Estimation

This section firstly introduces the working principle of AHIF, and then introduces the detailed process of estimating SOC based on the proposed synthetic algorithm.

A. Adaptive H-Infinity Filter

KF provides optimal state estimation by pursuing the minimum mean square error as the optimal estimation criterion [44], and requires accurate system models and statistical information of external interference signals beforehand. However, the statistical characteristics of noise and accurate system model are difficult to attain in practice, thus undoubtedly deteriorating the estimation accuracy. In this context, HIF is developed to cope with model uncertainty and external disturbance uncertainty of the system. Compared with KF, HIF does not entail noise statistics information in advance [45]. However, in HIF algorithms, it is assumed that the process and measurement noise covariance are constant; however, during SOC estimation, the noise covariance may vary with battery internal and surrounding operation conditions. Thus, to improve the performance of LSTM network, AHIF,

which can adjust the noise covariance dynamically, is employed to predict the SOC in this study. A standard linear time-varying discrete system can be formulated, as:

$$\begin{cases} X_{k+1} = A_k X_k + B_k U_k + \omega_k \\ Y_k = C_k X_k + D_k U_k + \nu_k \\ Z_k = L_k X_k \end{cases} \tag{13}$$

where X_k, Y_k and Z_k represent the state variable, the measurement variable with noise and the linear combination of estimation state; A_k and B_k mean the state transition matrix and control input matrix; C_k and D_k represent the measurement matrix and control output matrix; L_k is the user-defined matrix, which is set to unit matrix in this study; ω_k denotes the system noise; and ν_k indicates the measurement noise. The cost function of AHIF can be presented, as:

$$J = \frac{\sum_{k=0}^{K-1} \left\| Z_k - \hat{Z}_k \right\|_{S_k}^2}{\left\| X_0 - \hat{X}_0 \right\|_{P_0^{-1}}^2 + \sum_{k=0}^{K-1} \left(\left\| \omega_k \right\|_{Q_k^{-1}}^2 + \left\| \nu_k \right\|_{R_k^{-1}}^2 \right)} \tag{14}$$

where X_0 and $\hat{X}_0$ represent the initial value and initial set value of state quantity; P_0, Q_k, R_k and S_k are positive definite matrices. In fact, J is difficult to be minimized directly; and to tackle it, a certain boundary ε is proposed to assist in searching for the suboptimal value, that is:

$$J < \frac{1}{\varepsilon} \tag{15}$$

Combining (14) and (15), an updated cost function can be reformulated, as:

$$J = -\frac{1}{\varepsilon} \left\| X_0 - \hat{X}_0 \right\|_{P_0^{-1}}^2 + \sum_{k=0}^{K-1} \left\| Z_k - \hat{Z}_k \right\|_{S_k}^2 - \frac{1}{\varepsilon} \sum_{k=0}^{K-1} \left(\left\| \omega_k \right\|_{Q_k^{-1}}^2 + \left\| \nu_k \right\|_{R_k^{-1}}^2 \right) < 0 \tag{16}$$

since Z_k is a linear representation of X_k, now solving the optimization value of Z_k turns into finding the proper X_k that minimizes J. The recursive calculation procedure of AHIF is detailed as follows:

Step 1. Initialization

Set the initial value of X_0, Q_0, R_0, N, ε and calculate the initial mean $\hat{X}_0^+$ and covariance P_0^+, as:

$$\begin{cases} \hat{X}_0^+ = E(X_0) \\ P_0^+ = E\left[(X_0 - \hat{X}_0^+)(X_0 - \hat{X}_0^+)^T \right] \end{cases} \tag{17}$$

where X presents the state variable; Q denotes the system noise covariance; R means the measurement noise covariance; and N is the window size for covariance matching.

Step 2. Time update

1) Calculate the prior estimate of state:

$$\hat{X}_k^- = A_{k-1}\hat{X}_{k-1}^+ + B_{k-1}U_{k-1} \tag{18}$$

2) Calculate the prior estimate of error covariance:

$$P_k^- = A_{k-1}P_{k-1}^+ {A_{k-1}}^T + Q_{k-1} \tag{19}$$

3) Calculate the symmetric positive definite matrix update:

$$\bar{S}_k = L_k^T S_k L_k \tag{20}$$

Step 3. Measurement update

1) Condition judgment:

$$(P_k^-)^{-1} - \varepsilon \bar{S}_k + C_k^T R_k^{-1} C_k > 0 \tag{21}$$

2) Innovation update:

$$e_k = Y_k - C_k \hat{X}_k^- - D_k U_k \tag{22}$$

3) Adaptive estimation of measurement noise matrix calculation:

$$\hat{M}_k = \frac{1}{N} \sum_{i=k-N+1}^{k} e_i e_i^T, \hat{R}_k = \hat{M}_k - C_k P_k^- C_k^T \tag{23}$$

4) Gain matrix update:

$$G_k = A_k P_k^- (I - \varepsilon \bar{S}_k P_k^- + C_k^T R_k^{-1} C_k P_k^-)^{-1} C_k^T R_k^{-1} \tag{24}$$

5) Adaptive estimation of system noise matrix calculation:

$$\hat{Q}_k = K_k \hat{M}_k G_k^T \tag{25}$$

6) Measurement update of state estimate:

$$\hat{X}_k^+ = \hat{X}_k^- + G_k e_k \tag{26}$$

7) Measurement update of error covariance:

$$P_k^+ = P_k^- (I - \varepsilon \bar{S}_k P_k^- + C_k^T R_k^{-1} C_k P_k^-)^{-1} \tag{27}$$

where I represents the identity matrix. After presenting the principle of AHIF, the synthetic method for SOC estimation will be elaborated.

B. Synthetic SOC Estimation Method

The schematic of the proposed synthetic SOC estimation method based on LSTM and AHIF is depicted in Fig. 2. The whole process is mainly divided into four parts: data measurement, data processing, model training and test as well as filtering application. Firstly, the dynamic operation data are acquired. Then, the test data are processed and divided into two categories, i.e., training dataset and test dataset. Then, the LSTM is employed to excavate the veiled dependence between the measurement and SOC according to the training data, and then the trained model is applied to predict the rough SOC. Finally, to make the estimation results smoother and more reliable, the AHIF is implemented to further filter the output of LSTM.

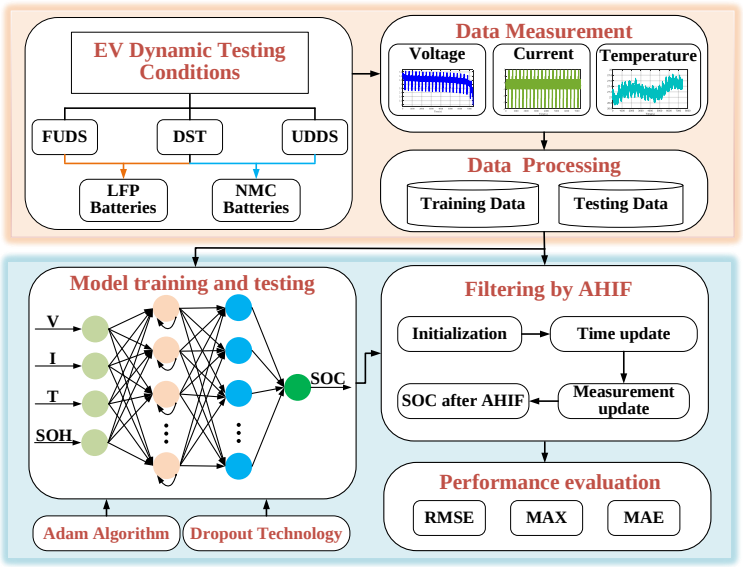

Fig. 2. The SOC estimation framework incorporating LSTM network and AHIF.

In the AHIF algorithm, the state function is based on the Ah integration method, and the LSTM model is chosen as the measurement function. The main task of AHIF is to eliminate the noise in the LSTM and renovate the SOC. The state and measurement functions can be formulated as:

$$\begin{cases} SOC_k = SOC_{k-1} + \dfrac{\eta_k I_k \Delta t}{3600Ca} + \omega_{k-1} \\ SOC_{L,k} = SOC_k + v_k \end{cases} \tag{28}$$

where SOC_k and $SOC_{L,k}$ denote the output values by the Ah integration method and LSTM model at time step k, respectively; η_k represents the coulomb efficiency; I indicates the current, which is positive for charging and negative for discharging; Δt means the sampling time interval; Ca is the battery rated discharge capacity. Accordingly, the parameters of (13) can be determined, as:

$$\begin{cases} X_k = SOC_k \\ U_k = I_k \\ B = \eta_k \Delta t / 3600Ca; \\ Y_k = SOC_{L,k} \end{cases} \tag{29}$$

In addition, A and C are the identity matrix, and D is the zero matrix. Moreover, the battery capacity highly depends on environment temperature and aging state. For easier calculation, a five-order polynomial equation, as shown in (30), is employed to fit the relationship between the maximum discharge capacity and temperature, and the measured and fitted results are plotted in Fig. 3. The maximum discharge capacity at different temperature is obtained by the calibration test. According to the specifications, the test is conducted during -10 ℃ to 50 ℃ with the interval of 10 ℃. In each test, the experimental procedures are briefly described as follows. Firstly, a constant current (CC) charging strategy with the current of 0.5C is conducted, and when the voltage reaches 4.2 V, the constant voltage (CV) charging strategy is activated until the current decreases to 0.02C. After shelving for 2 hours, the battery is discharged with 1C current, until the voltage drops to 2.75 V. The above steps are repeated for three times, and the average capacity value is considered as the real maximum capacity at the current temperature.

$$Q_n(T) = 2.667\times10^{-09}T^5 - 4.258\times10^{-07}T^4 + 2.555\times10^{-05}T^3 - 0.00094T^2 + 0.03448T + 3.34011 \tag{30}$$

where T denotes the battery temperature. Note that for ease of calculation, it is assumed that the capacity of the aged battery is known in advance due to the enabling SOH prediction techniques [46, 47].

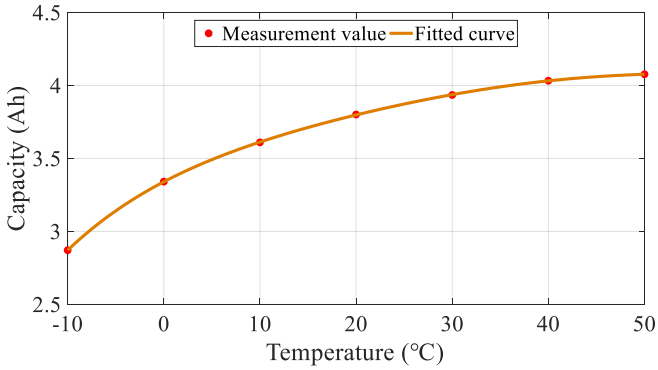

Fig. 3. The initial capacity at different temperatures.

In the following section, the estimation performance of the proposed method will be examined based on a series of experimental validations.

IV. Results and Discussions

In this section, four critical hyper-parameters of the LSTM network are firstly determined, and then the data of LFP batteries and NCM batteries under different operating temperatures are exerted to examine the performance and generalization ability of the proposed method. Next, by comparing with different methods, the robustness and convergence ability of the proposed method under incorrect initial SOC are further validated. Finally, the feasibility of the proposed method on aged batteries is verified.

A. Hyper-Parameter Selection

The test target in this and next part is the LFP batteries with the same SOH (100%), of which the cut-off voltage is 2/3.6 V, and the rated capacity is 2.3 Ah. To collect sufficient data for model training and testing of the LSTM network, two dynamic testing profiles including federal urban driving schedule (FUDS) and dynamic stress test (DST) under different temperatures are performed, and the sampling interval is set to 1 s in this study. The FUDS cycle imitates urban driving conditions, while DST accounts for a variety of current steps with different lengths and amplitudes [48]. Fig. 4 shows the current and voltage of FUDS and DST test. The batteries are repeatedly experimented at -10 ℃ to 50 ℃ with 10 ℃ as an increase interval and at room temperature (27 ℃), respectively.

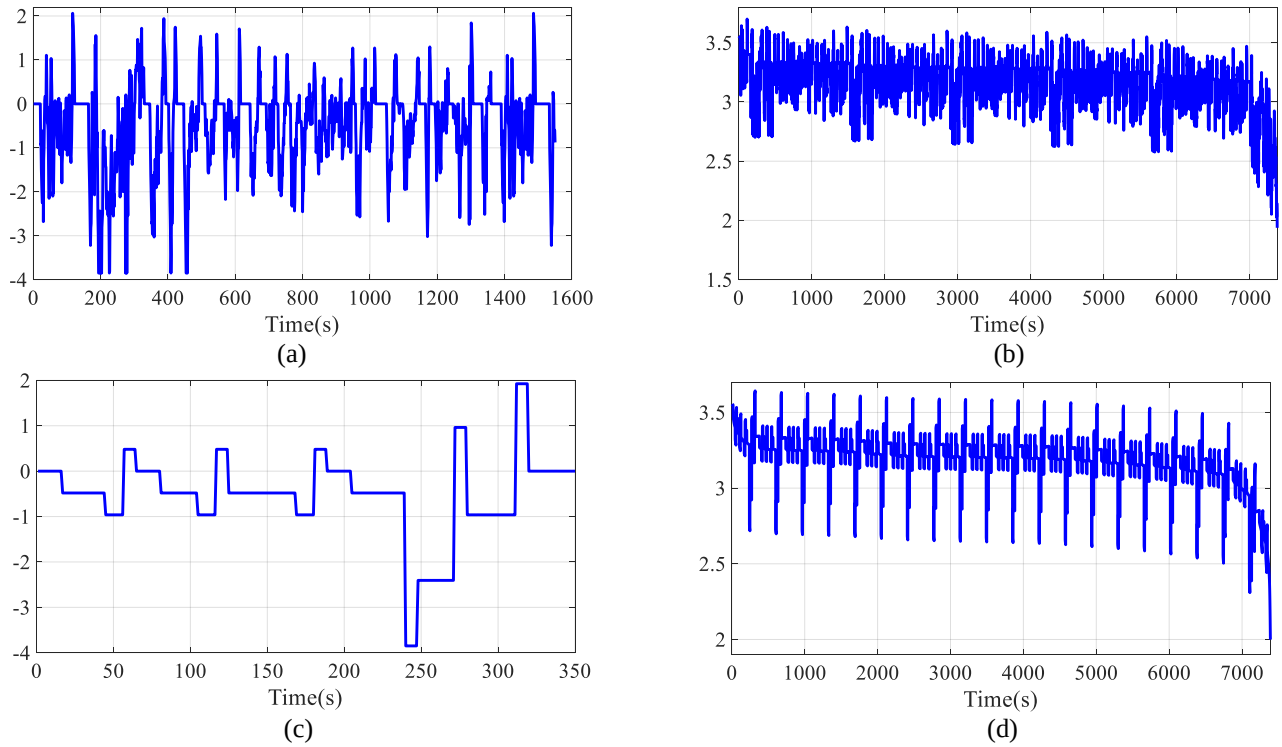

Fig. 4. Current and temperature change of training data and test data. (a) Training data; (b) Test data; (c) Current profiles of DST; (d) Measured voltage of DST.

The performance of LSTM network on SOC estimation is significantly affected by four key hyper-parameters including the hidden node, hidden LSTM layer, batch size and training epoch. However, the search space of the hyper-parameters increases exponentially with the increase of hidden nodes and layers [29], making it challenging and time-consuming to find the proper hyper-parameters. To trade off model accuracy and computational efficiency, this study starts to search the hyper-parameters of LSTM network in a small range through the stepwise search method [49]. By this manner, precise battery modeling and burdensome model parameter identification tasks that are imperative in traditional observers or filters can be omitted, thus improving the model training and application efficiency. For LFP batteries, the training data of LSTM are collected at -10 ℃, 0 ℃, 10 ℃, 20 ℃, 30 ℃, 40 ℃ and 50 ℃ under the FUDS experiment. The data collected from the DST test at 27 ℃ are implemented to evaluate the model performance.

The first hyper-parameter waiting to be determined is the number of nodes in the hidden layer of LSTM. Table I shows the test results in terms of RMSE, MAX and MAE with the nodes number varying within [8, 20, 30, 36, 40, 50, 60]. It can be clearly observed that more nodes can achieve better estimation accuracy. When 36 nodes are offered, 29%, 27% and 32% reduction in RMSE, MAX and MAE error can be attained, compared with

those by 8 nodes. However, increasing the node number from 36 to 60 will lead to the increase in RMSE, MAX and MAE due to over-fitting. To balance all the criteria, 36 hidden nodes are preferred in this study.

Next, four networks with different hidden layers are constructed according to the number of hidden nodes determined above, and then the hidden layer number is selected according to their performance. The details of these four networks and their prediction results are listed in Table II. Although the total numbers of hidden nodes in the four networks remain the same, the RMSE, MAX and MAE of networks 2 to 4 show an increasing trend, compared with those by network 1. The reason can be explained as follows. Since there are only a few input variables in the network, over complex network structures with more hidden layers will also lead to over-learning and over-fitting. In other words, we can conclude that one hidden layer is enough to estimate SOC.

Table I. Results of SOC estimation with different numbers of hidden node.

Hidden nodes	8	20	30	36	40	50	60
RMSE (%)	3.98	3.97	3.56	2.83	3.96	4.13	4.77
MAX (%)	18.63	17.83	16.34	13.65	16.51	20.02	20.48
MAE (%)	3.11	2.93	2.48	2.12	2.81	2.82	3.33

Table II. Results of SOC estimation with different numbers of LSTM hidden layers.

Network	Hidden layers	Hidden nodes	RMSE (%)	MAX (%)	MAE (%)
1	1	36	2.83	13.65	2.12
2	2	18-18	3.33	17.73	2.24
3	3	12-12-12	4.15	17.9	2.99
4	4	9-9-9-9	3.75	20.94	2.45

The third critical hyper-parameter is the batch size (BS), which determines the number of training data in a single batch and decides the direction of gradient descent. Since the dataset used in this paper is relatively large, the small batch gradient descent method is herein adopted to improve the performance of LSTM model [50]. To choose an appropriate BS value, the research scope of BS is [8, 16, 32, 64, 128, 256, 512, 1024], and the corresponding RMSE, MAX and MAE are tabulated in Table III. As can be found, when BS equals 128, the RMSE and MAX reach the minimum value 2.83% and 13.65%, while MAE reaches 2.12%, which is slightly higher than the minimum value (2%), meeting the practical requirements. As such, the BS is set to 128 after performance evaluation.

Finally, the number of training epochs is determined. Table IV shows the results of training time, RMSE, MAE and MAX with different epochs. It is apparent that the training time increases with the increase of training

epochs, while the variation trend of RMSE, MAE and MAX are different. When the epoch is 100, although the RMSE and MAE both reach the minimum value, the MAX exceeds 20%, and the training time is about 73.82 minutes. The MAX reaches the minimum value when the epoch is 50, and in this case the RMSE and MAE values are slightly higher than the minimum value, whereas the training time is only about one third of that when the epoch is 100. Given the trade-off between test precision and training time, 50 is a preferable choice, and as such the number of training epoch is determined.

By means of the above four steps, a well-tuned LSTM model, including one hidden layer, 36 hidden nodes, 128 BS and 50 training epochs, is determined and then applied to estimate SOC. The optimized LSTM network cannot only attain the satisfactory estimation accuracy, but also show high computational efficiency. The training time on a laptop computer with i5-10210U CPU is less than 25 minutes, and the average calculation time for each step is 0.064 ms, meeting the real-time application requirement of the proposed algorithm.

Table III. Results of SOC estimation with different numbers of batch size.

Batch size	8	16	32	64	128	256	512	1024
RMSE (%)	3.03	3.24	3.8	3.41	2.83	4.43	4.53	6.26
MAX (%)	30.05	26.51	18	17.5	13.65	15.16	23.53	27.23
MAE (%)	2	2.32	2.66	2.38	2.12	3.42	3.34	4.69

Table IV. Results of SOC estimation with different numbers of epoch.

Epoch	5	10	25	40	50	60	70	80	90	100
Training time (min)	2.07	4.13	10.22	16.28	24.8	27.73	28.94	37.77	59.33	73.82
RMSE (%)	5.46	4.89	4.57	3.65	2.83	3.08	3.83	3.87	3.09	2.64
MAX (%)	24.92	23.5	21.97	13.67	13.65	14.89	18.91	15.65	14.98	21.58
MAE (%)	4.2	3.59	3.42	2.96	2.12	2.28	2.86	2.77	2.18	1.81

B. SOC Estimation at Different Temperature

Temperature is one of the main factors affecting the estimation precision of SOC, and accurate and reliable SOC estimation in a wide temperature range is critical for efficient operation of LIBs in EVs. The performance of the LSTM model is evaluated by the DST data at -10 ℃, 0 ℃, 10 ℃, 20 ℃, 30 ℃, 40 ℃, 50 ℃ and 27 ℃, respectively. Note that 27 ℃ experimental data are not included in the training. Fig. 5 displays the prediction results of SOC and the corresponding estimation error at -10 ℃ (low temperature), 27 ℃ and 50 ℃ (high temperature), respectively. Moreover, the single LSTM model without AHIF is also applied to estimate SOC for performance evaluation.

The results manifest that the performance of single-LSTM method at -10 ℃ is unsatisfactory, and the main reason lies in the sharp increase of polarization when the battery works at low temperature. At other temperatures, the single-LSTM method can track the variation of SOC efficiently, and the RMSE and MAE are less than 4% and 3.1%, respectively. However, the MAX is higher than 10% in most cases (except 40 ℃ experiment), indicating that the results are not stable and fluctuate dramatically. As can be seen from Fig. 5, large estimation deviation emerges when SOC varies in the range of 30% to 80%. This is mainly caused by the flat voltage plateau existing in the discharge voltage curve of LFP batteries, and small voltage error or noise can lead to large SOC estimation deviation. In addition, due to polarization, larger estimation error also occurs in low SOC area. In short, although the single-LSTM method highlights acceptable generalization ability for different driving cycles and temperatures, the estimated results cannot meet the requirements of practical applications, and therefore it still needs to be improved. Fig. 5 shows the results by the proposed synthetic method. As can be found, the filtered SOC curve can accurately and stably track the reference curve in the full range at low and high temperatures. Moreover, the problems of large SOC estimation error appearing in low SOC and voltage platform area can also be properly tackled. Table V compares the prediction results of the single-LSTM method and the proposed synthetic method at different temperatures. It can be found that the proposed method can lead to remarkable reduction of RMSE, MAX and MAE. To be specific, the RMSE is reduced from 7.52% to 1.09% at -10 ℃, from 2.83% to 0.22% at 27 ℃ and from 2.83% to 0.73% at 50 ℃; and in particular, the MAX is dramatically lowered from 30.50% to 1.3% at -10 ℃, from 13.65% to 0.89% at 27 ℃ and from 10.73% to 1.15% at 50 ℃. Similar decrements also happen to the MAE. To sum up, the RMSE, MAX and MAE are all restricted within 2% after applying the AHIF, revealing that the proposed estimation framework can well adapt to wide temperature conditions with reliable and satisfactory prediction accuracy.

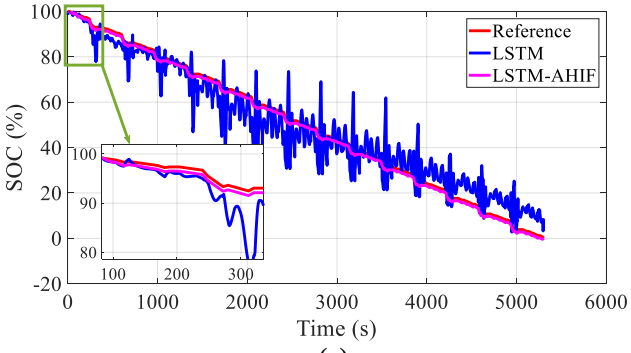

(a)

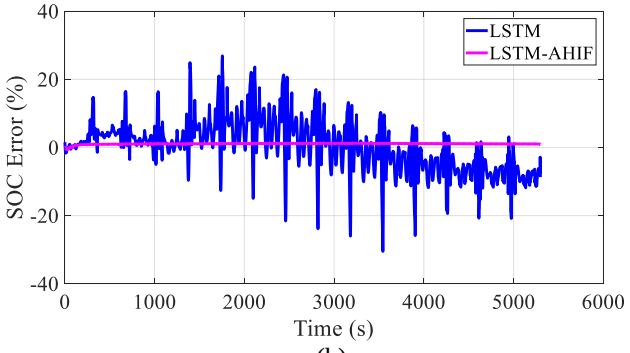

(b)

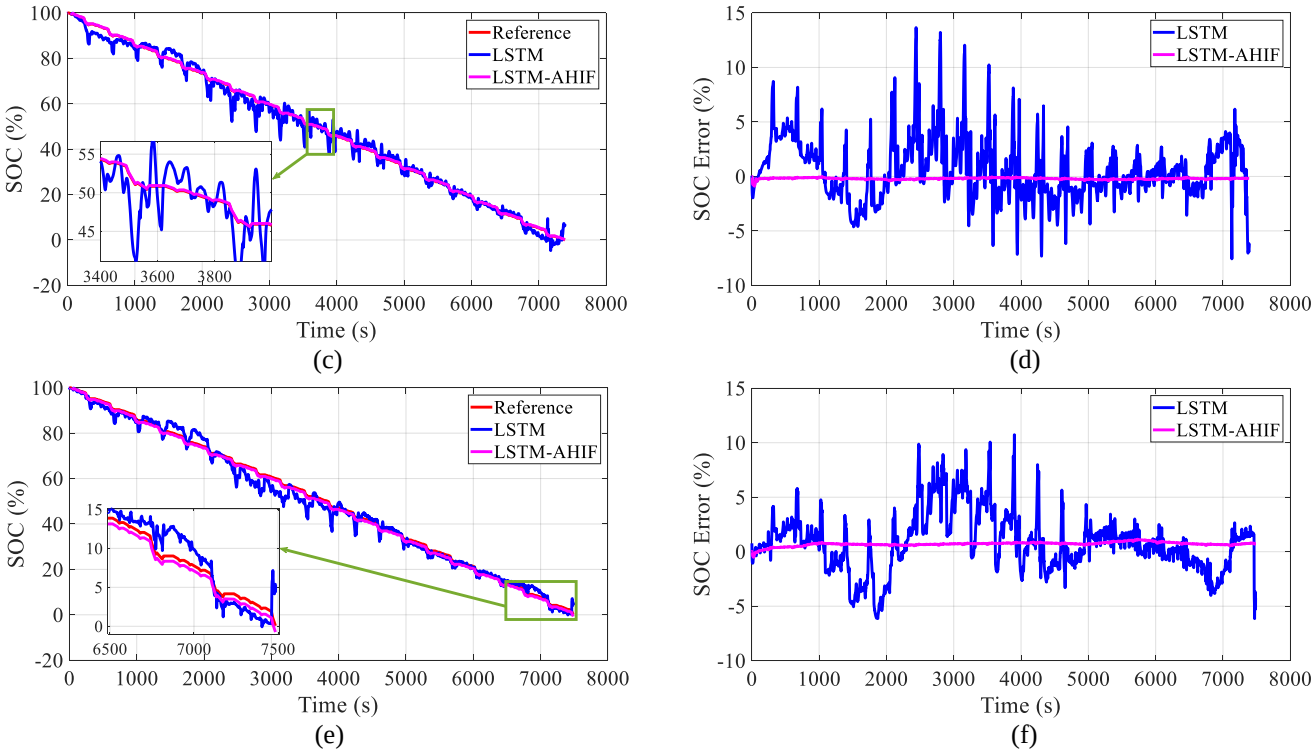

Fig. 5. SOC estimation results at different temperatures. (a) SOC result at -10 ℃ and (b) SOC error at -10 ℃; (c) SOC result at 27 ℃; (d) SOC error at 27 ℃; (e) SOC result at 50 ℃; (f) SOC error at 50 ℃.

Table V. Evaluation results of different temperatures.

Temperature (℃)	RMSE (%)		MAX (%)		MAE (%)	
	LSTM	LSTM-AHIF	LSTM	LSTM-AHIF	LSTM	LSTM-AHIF
-10	7.52	1.09	30.50	1.30	5.84	1.08
0	3.62	0.52	13.61	1.33	2.84	0.51
10	3.36	0.37	17.03	1.26	2.57	0.31
20	3.91	0.47	18.42	2	3.08	0.35
27	2.83	0.22	13.65	0.89	2.12	0.21
30	2.89	0.77	13.14	1.54	2.32	0.72
40	3.14	1.26	8.57	1.92	2.36	1.18
50	2.83	0.73	10.73	1.15	2.13	0.71

C. SOC Estimation under Dynamic Time-Varying Temperature Conditions

To explore the generalization of the proposed method, another type of batteries, i.e., NCM battery, is experimented to validate the SOC estimation performance in this part. It is worth mentioning that the hyper-parameters of LSTM network remain the same as before. In the battery testing process, the NCM batteries with the rated capacity of 4 Ah are fully charged with the CC-CV scheme, followed by the rest for 2 hours; then the battery is discharged under dynamic working conditions until the voltage dropped to the cut-off voltage of 2.75 V. It is worth noting that under varying temperature conditions, the maximum capacity at current temperature is firstly obtained through the interpolation between the maximum discharge capacity and temperature, as expressed in (30), and then the reference SOC is calculated according to the Ah integration method.

It can be found from previous discussions that the proposed method raises satisfactory estimation performance when validated under constant operation temperatures. However, in practice, it is almost impossible for batteries to work at a constant temperature. Hence, the dynamic temperature experiment needs to be performed to further verify the generalization and robustness of the proposed method. Since the type of test battery is different, the LSTM model needs to be retrained, and the training data are re-selected. The training dataset of NCM batteries is derived from the DST and urban dynamometer driving schedule (UDDS) cycle, and the current profile, temperature variation and SOH are shown in Fig. 6 (a). The test data are mainly obtained through the FUDS experiment under four time-varying temperature conditions, as sketched in Fig. 6 (b). Obviously, the temperature variation of the training dataset and the test dataset is distinctly different. The estimation is conducted under four datasets, namely data 1, data 2, data 3 and data 4; and the results are shown in Fig. 6 (c) to (j). The data 1 mainly simulates the battery's operation in the high temperature ranging from 31 ℃ to 50 ℃; the data 2 accounts for the temperature decreases from high temperature (40 ℃) and low temperature (17 ℃); and the main purpose of data 3 and 4 are to validate the performance under varying conditions changing from low temperature (9 ℃) to high temperature (52 ℃) and from high temperature (52 ℃) to low temperature (12 ℃).

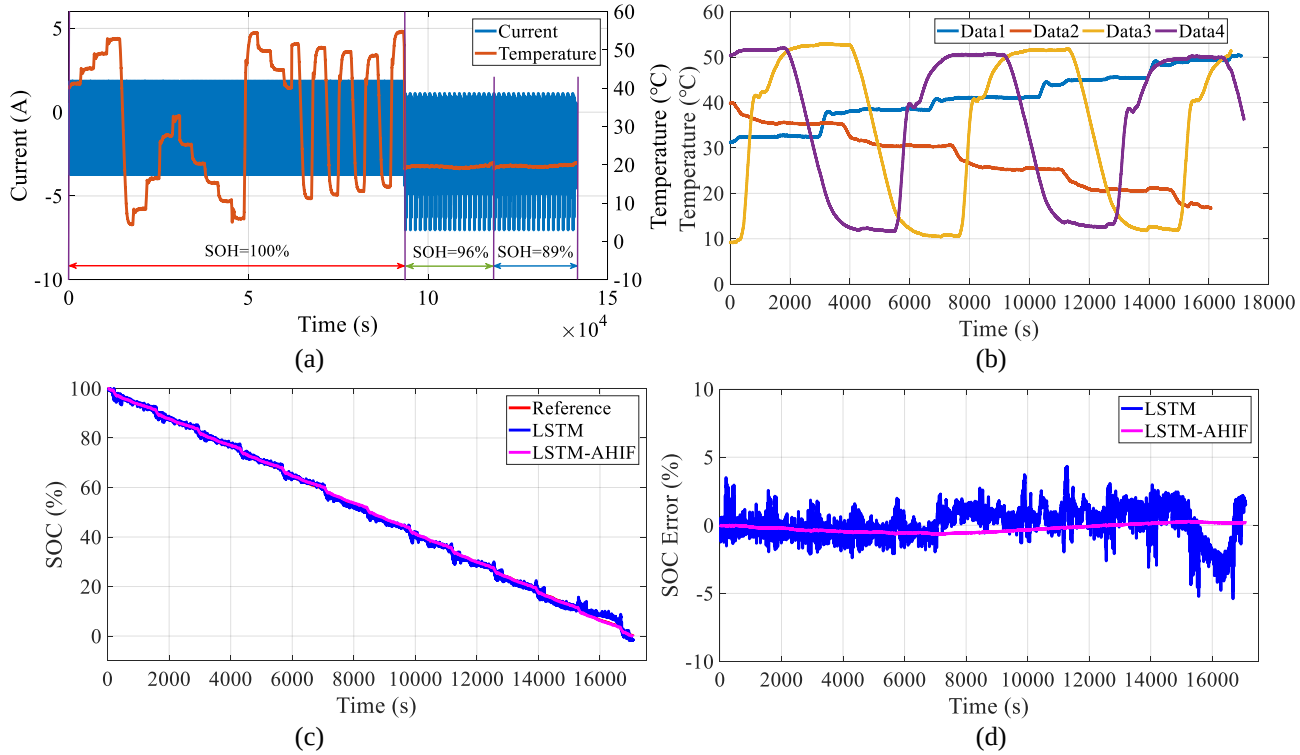

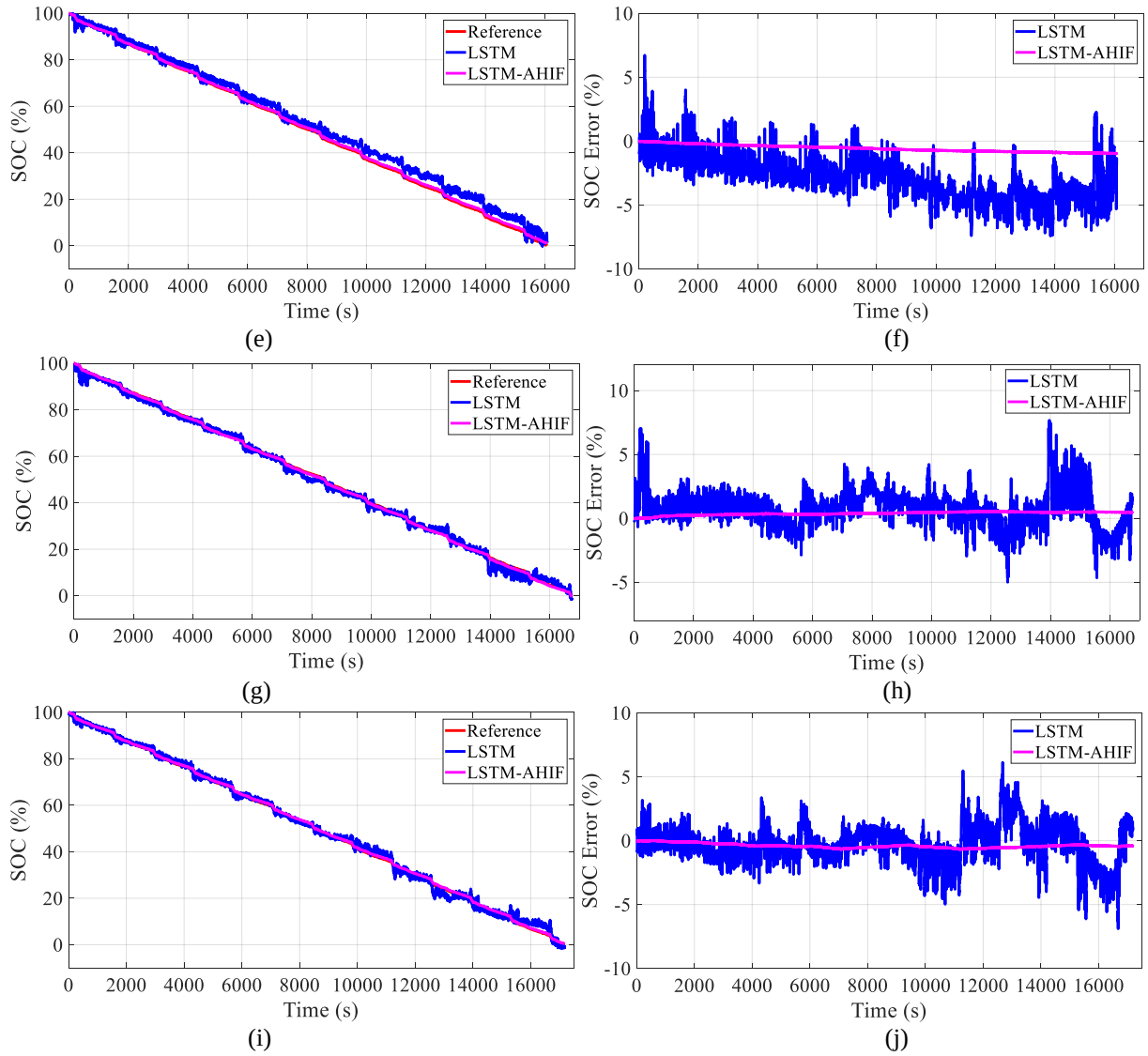

Fig. 6. SOC estimation results under time-varying temperature. (a) Current, temperature and SOH variation of training dataset; (b) Temperature variation of test dataset; (c), (e), (g) and (i) SOC estimation result of data 1, 2, 3 and 4; (d), (f), (h) and (j) SOC estimation error of data 1, 2, 3 and 4.

As can be found from Fig. 6 (c) to (j), although the single-LSTM method can track the reference SOC curve, obvious fluctuations still exist, especially when SOC is lower than 40%. Instead, the proposed method can effectively improve the SOC estimation accuracy, and the variation curve can track the reference value smoothly and accurately. Table VI detailed all the criteria of the single-LSTM and the proposed method in all validations. It can be found that the RMSE, MAX and MAE by the single-LSTM method can be controlled within 3.25%, 7.67% and 2.93%, respectively. While the RMSE by the proposed method is less than 0.63%, much less than that by single-LSTM method; and the MAX and MAE by the proposed method are lower than 1% and 0.57%, indicating that the proposed method highlights strong robustness against different battery types and superior estimation accuracy under dynamic time-varying temperature conditions.

Table VI. Evaluation results of dynamic time-varying temperature.

Dataset	RMSE (%)		MAX (%)		MAE (%)	
	LSTM	LSTM-AHIF	LSTM	LSTM-AHIF	LSTM	LSTM-AHIF
Data 1	1.2	0.36	5.39	0.68	0.98	0.3
Data 2	3.25	0.63	7.43	1	2.93	0.57
Data 3	1.6	0.4	7.67	0.55	1.25	0.39
Data 4	1.46	0.43	6.89	0.69	1.13	0.4

D. SOC Estimation with Different Methods

To further evaluate the performance of the proposed method, two mainstream SOC estimation methods, i.e., EKF and AEKF are applied based on the first-order equivalent circuit model (ECM), and both algorithms are hereinafter referred to as ECM-EKF and ECM-AEKF. GA is employed to identify the model parameters of lithium-ion batteries. In addition, the LSTM-HIF method is also employed. The UDDS data collected at 20 ℃ are regarded as the test target, and currently the battery SOH is 100%. Furthermore, inaccurate initial SOC is imposed to evaluate the convergence performance of different methods. The actual initial SOC value is 100%, and the initial value in the estimation algorithm is mistakenly set to 80%, 60%, 40% and 20%. The convergence time, RMSE and MAE are taken as the evaluation indexes.

Fig. 7 depicts the SOC estimation results and error when the initial SOC value is incorrectly set to 40%. As can be observed, all the methods enable the SOC to compensate the large initial difference and converge to the true value. Table VII provides the statistical results in terms of the convergence speed, RMSE and MAE of different methods with different initial SOC values. Obviously, the proposed method and LSTM-HIF method lead to better convergence performance, and under all cases, the convergence time is restricted within 12 s. By contrast, the convergence time by the EKF and AEKF algorithms rises greatly with the increase of initial SOC error, even reaching 441 s, which is nearly 40 times than that by the proposed method under the same settings. It can also be found that the proposed method raises the least SOC estimation error in all cases, and the RMSE and MAE are less than 1.73% and 1.4%, respectively. In brief, compared with the traditional model-based filtering methods and LSTM-HIF method, the proposed method exhibits satisfactory estimation accuracy and remarkable convergence speed when encountered with incorrect initial SOC values.

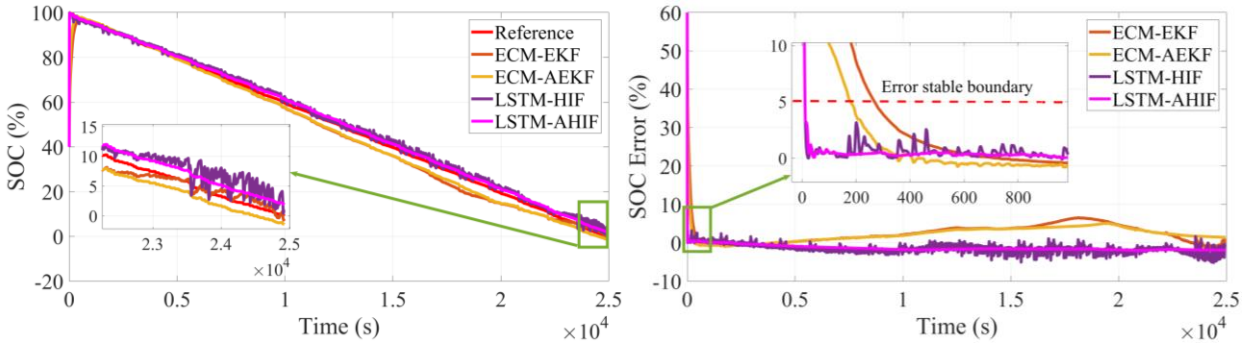

(a) (b)

Fig.7. SOC estimation when initial SOC=40% using different method. (a) SOC profiles; (b) SOC errors.

Table VII. Estimation results with inaccurate initial SOC.

Initial SOC (%)	Convergence time (s)				RMSE (%)				MAE (%)			
	ECM-EKF	ECM-AEKF	LSTM-HIF	LSTM-AHIF	ECM-EKF	ECM-AEKF	LSTM-HIF	LSTM-AHIF	ECM-EKF	ECM-AEKF	LSTM-HIF	LSTM-AHIF
100	0	0	0	0	2.75	2.18	1.74	0.71	2.22	1.91	1.57	0.59
80	88	25	8	8	3.15	2.73	1.88	1.08	2.5	2.31	1.61	0.93
60	177	64	10	10	3.36	2.81	1.92	1.11	2.56	2.33	1.61	0.9
40	269	181	11	11	3.88	3.21	1.99	1.64	2.67	2.42	1.61	1.4
20	441	381	12	12	5.5	5.02	2.08	1.73	2.93	2.72	1.62	1.38

E. SOC Estimation with Aged Batteries

In this part, the application prospect of the proposed method will be examined by using the aged test data. After the battery is fully charged according to the CC-CV strategy, the UDDS current is imposed at 20 ℃ until the voltage drops to 2.75 V. Here, the SOH of test battery selected for validation is 87%. The SOC estimation results is illustrated in Fig. 8. As can be seen, the LSTM network can successfully reflect the mapping between SOC and the measured voltage, current, temperature as well as the predicted SOH at the untrained aging state, manifesting its extendibility when the training data are scarce. The RMSE and MAE of SOC estimated by the single-LSTM method are 2.41% and 1.95%, respectively; whereas the MAX is 7.71%, revealing that the estimation results fluctuate dramatically. Thus, we can conclude that the single-LSTM model cannot predict the SOC accurately when the battery is aged. However, the AHIF can be applied to eliminate the unwanted noises outputted by the LSTM network. The proposed synthetic method based on LSTM and AHIF achieves quite low error when the battery is aged; and the RMSE, MAX and MAE are 0.7%, 1.25% and 0.62%, which are respectively reduced by 67.29%, 83.79% and 68.21%, compared with those by the single-LSTM method. In short, the results clearly manifest the effectiveness of the proposed method even in the aged batteries.

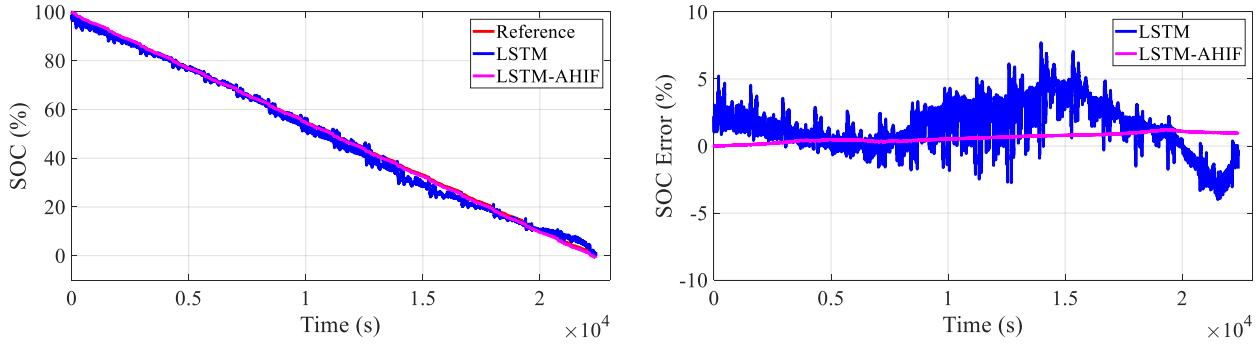

Fig. 8. SOC estimation results at aging batteries. (a) SOC estimation of 87% SOH; (b) SOC estimation error of 87% SOH.

To conclude, the precision, convergence speed, robustness, extendibility and real-time application capacity of the proposed synthetic algorithm are fully justified from various perspectives including different battery types, varying current, high and low temperature as well as different aged states.

V. Conclusion

This paper investigates the influence of time sequence factors on state of charge estimation for lithium-ion batteries, and proposes a synthetic estimation method incorporating long short-short term memory network and adaptive H-infinity filter. The battery voltage, current, temperature and SOH are hired as the input of the long short-short term memory network, and the adaptive H-infinity filter is applied to eliminate the output noise of the long short-short term memory network, thereby achieving accurate and stable state of charge estimation. The feasibility and superior performance of the proposed method is verified on different types of batteries under dynamic working conditions and aging state.

For lithium iron phosphate batteries, the experimental results show that the proposed method can accurately estimate state of charge in a wide temperature range from -10 ℃ to 50 ℃, and the root mean square error, maximum absolute error and mean absolute error of the estimation results are restricted within 1.26%, 2% and 1.18%, respectively. For lithium nickel cobalt manganese batteries, the experimental results reveal that even the batteries work under dynamic time-varying temperature conditions, the root mean square error, maximum absolute error and mean absolute error of estimation results by the proposed method can also be restrained within 0.63%, 1%, and 0.57%. Compared with traditional methods (extended Kalman filter and adaptive extended Kalman filter) and H-infinity filter with the built long-short term memory model, the proposed method leads to stronger robustness and higher estimation accuracy, even when the battery capacity is degraded. Moreover, the calculation

time of each step of the proposed algorithm is less than 1 millisecond and is therefore feasible for real-time application. In summary, the proposed algorithm is proved to be an ideal state of charge estimation method with satisfactory performance after extensive validations.

In addition, this paper is dedicated to state of charge estimation of single battery cell; whereas in practical applications, a variety of cells are often grouped to form battery modules or packs. Therefore, in our future work, the influence due to cell inconsistency and state of health difference of cells will be investigated to improve state of charge estimation performance of battery module or pack.

ACKNOWLEDGEMENTS

This work was supported in part by the National Key R&D Program of China (No. 2019YFC1907901), in part by the National Natural Science Foundation of China (No. 61763021 and 51775063), and in part by the EU-funded Marie Skłodowska-Curie Individual Fellowships Project under Grant 845102-HOEMEV-H2020-MSCA-IF-2018.

REFERENCES

[1] W. Xu, J. Xu, J. Lang, and X. Yan, "A Multi-Timescale Estimator for Lithium-Ion Battery State of Charge and State of Energy Estimation Using Dual H Infinity Filter," *IEEE Access,* vol. 7, pp. 181229-181241, 2019, doi: 10.1109/ACCESS.2019.2959396.

[2] M. A. Hannan, M. H. Lipu, A. Hussain, and A. Mohamed, "A review of lithium-ion battery state of charge estimation and management system in electric vehicle applications: Challenges and recommendations," *Renewable and Sustainable Energy Reviews,* vol. 78, pp. 834-854, 2017.

[3] X. Shu, G. Li, J. Shen, W. Yan, Z. Chen, and Y. Liu, "An adaptive fusion estimation algorithm for state of charge of lithium-ion batteries considering wide operating temperature and degradation," *Journal of Power Sources,* vol. 462, p. 228132, 2020/06/30/ 2020, doi: https://doi.org/10.1016/j.jpowsour.2020.228132.

[4] E. Chemali, P. J. Kollmeyer, M. Preindl, and A. Emadi, "State-of-charge estimation of Li-ion batteries using deep neural networks: A machine learning approach," *Journal of Power Sources,* vol. 400, pp. 242-255, 2018.

[5] C. Chen, R. Xiong, R. Yang, W. Shen, and F. Sun, "State-of-charge estimation of lithium-ion battery using an improved neural network model and extended Kalman filter," *Journal of Cleaner Production,* vol. 234, pp. 1153-1164, 2019.

[6] X. Ding, M. Du, C. Duan, H. Guo, R. Xiong, J. Xu, J. Cheng, and P. C. k. Luk, "Analytical and Experimental Evaluation of SiC-Inverter Nonlinearities for Traction Drives Used in Electric Vehicles," *IEEE Transactions on Vehicular Technology,* vol. 67, no. 1, pp. 146-159, 2018, doi: 10.1109/TVT.2017.2765670.

[7] Z. Chen, L. Yang, X. Zhao, Y. Wang, and Z. He, "Online state of charge estimation of Li-ion battery based on an improved unscented Kalman filter approach," *Applied Mathematical Modelling,* vol. 70, pp. 532-544, 2019.

[8] Y. Bi and S.-Y. Choe, "An adaptive sigma-point Kalman filter with state equality constraints for online state-of-charge estimation of a Li (NiMnCo) O2/Carbon battery using a reduced-order electrochemical model," *Applied Energy,* vol. 258, p. 113925, 2020.

[9] A. Gismero, E. Schaltz, and D.-I. Stroe, "Recursive State of Charge and State of Health Estimation Method for Lithium-Ion Batteries Based on Coulomb Counting and Open Circuit Voltage," *Energies,* vol. 13, no. 7, p. 1811, 2020.

[10] R. Xiong, Q. Yu, and C. Lin, "A novel method to obtain the open circuit voltage for the state of charge of lithium ion batteries in electric vehicles by using H infinity filter," *Applied energy,* vol. 207, pp. 346-353, 2017.

[11] U. Westerhoff, T. Kroker, K. Kurbach, and M. Kurrat, "Electrochemical impedance spectroscopy based estimation of the state of charge of lithium-ion batteries," *Journal of Energy Storage,* vol. 8, pp. 244-256, 2016.

[12] P. Shrivastava, T. K. Soon, M. Y. I. B. Idris, and S. Mekhilef, "Overview of model-based online state-of-charge estimation using Kalman filter family for lithium-ion batteries," *Renewable and Sustainable Energy Reviews,* vol. 113, p. 109233, 2019.

[13] D. N. How, M. Hannan, M. H. Lipu, and P. J. Ker, "State of charge estimation for lithium-ion batteries using model-based and data-driven methods: A review," *IEEE Access,* vol. 7, pp. 136116-136136, 2019.

[14] X. Shu, G. Li, J. Shen, Z. Lei, Z. Chen, and Y. Liu, "An adaptive multi-state estimation algorithm for lithium-ion batteries incorporating temperature compensation," *Energy,* p. 118262, 2020.

[15] J. Peng, J. Luo, H. He, and B. Lu, "An improved state of charge estimation method based on cubature Kalman filter for lithium-ion batteries," *Applied Energy,* vol. 253, p. 113520, 2019.

[16] X. Chen, H. Lei, R. Xiong, W. Shen, and R. Yang, "A novel approach to reconstruct open circuit voltage for state of charge estimation of lithium ion batteries in electric vehicles," *Applied Energy*, vol. 255, p. 113758, 2019.
[17] L. Sun, G. Li, and F. You, "Combined internal resistance and state-of-charge estimation of lithium-ion battery based on extended state observer," *Renewable and Sustainable Energy Reviews*, vol. 131, p. 109994, 2020.
[18] Y. Xu, M. Hu, A. Zhou, Y. Li, S. Li, C. Fu, and C. Gong, "State of charge estimation for lithium-ion batteries based on adaptive dual Kalman filter," *Applied Mathematical Modelling*, vol. 77, pp. 1255-1272, 2020.
[19] M. Zhang, K. Wang, and Y.-t. Zhou, "Online State of Charge Estimation of Lithium-Ion Cells Using Particle Filter-Based Hybrid Filtering Approach," *Complexity*, vol. 2020, 2020.
[20] F. Yang, Y. Xing, D. Wang, and K.-L. Tsui, "A comparative study of three model-based algorithms for estimating state-of-charge of lithium-ion batteries under a new combined dynamic loading profile," *Applied energy*, vol. 164, pp. 387-399, 2016.
[21] L. Zhi, Z. Peng, W. Zhifu, S. Qiang, and R. Yinan, "State of charge estimation for Li-ion battery based on extended Kalman filter," *Energy Procedia*, vol. 105, pp. 3515-3520, 2017.
[22] Y. Wang and Z. Chen, "A framework for state-of-charge and remaining discharge time prediction using unscented particle filter," *Applied Energy*, vol. 260, p. 114324, 2020.
[23] C. Lin, H. Mu, R. Xiong, and W. Shen, "A novel multi-model probability battery state of charge estimation approach for electric vehicles using H-infinity algorithm," *Applied Energy*, vol. 166, pp. 76-83, 2016.
[24] G. Liu, C. Xu, K. Jiang, and K. Wang, "State of charge and model parameters estimation of liquid metal batteries based on adaptive unscented Kalman filter," *Energy Procedia*, vol. 158, pp. 4477-4482, 2019.
[25] C. Chen, R. Xiong, and W. Shen, "A Lithium-Ion Battery-in-the-Loop Approach to Test and Validate Multiscale Dual H Infinity Filters for State-of-Charge and Capacity Estimation," *IEEE Transactions on Power Electronics*, vol. 33, no. 1, pp. 332-342, 2018, doi: 10.1109/TPEL.2017.2670081.
[26] C. Huang, Z. Wang, Z. Zhao, L. Wang, C. S. Lai, and D. Wang, "Robustness evaluation of extended and unscented Kalman filter for battery state of charge estimation," *Ieee Access*, vol. 6, pp. 27617-27628, 2018.
[27] T. Zahid, K. Xu, W. Li, C. Li, and H. Li, "State of charge estimation for electric vehicle power battery using advanced machine learning algorithm under diversified drive cycles," *Energy*, vol. 162, pp. 871-882, 2018.
[28] X. Shu, G. Li, J. Shen, Z. Lei, Z. Chen, and Y. Liu, "A uniform estimation framework for state of health of lithium-ion batteries considering feature extraction and parameters optimization," *Energy*, vol. 204, p. 117957, 2020/08/01/ 2020, doi: https://doi.org/10.1016/j.energy.2020.117957.
[29] D. N. How, M. Hannan, M. H. Lipu, K. S. Sahari, P. J. Ker, and K. M. Muttaqi, "State-of-Charge Estimation of Li-ion Battery in Electric Vehicles: A Deep Neural Network Approach," *IEEE Transactions on Industry Applications*, 2020.
[30] L. Kang, X. Zhao, and J. Ma, "A new neural network model for the state-of-charge estimation in the battery degradation process," *Applied Energy*, vol. 121, pp. 20-27, 2014/05/15/ 2014, doi: https://doi.org/10.1016/j.apenergy.2014.01.066.
[31] H. Chaoui and C. C. Ibe-Ekeocha, "State of charge and state of health estimation for lithium batteries using recurrent neural networks," *IEEE Transactions on vehicular technology*, vol. 66, no. 10, pp. 8773-8783, 2017.
[32] J. Schmidhuber and S. Hochreiter, "Long short-term memory," *Neural Comput*, vol. 9, no. 8, pp. 1735-1780, 1997.
[33] E. Chemali, P. J. Kollmeyer, M. Preindl, R. Ahmed, and A. Emadi, "Long short-term memory networks for accurate state-of-charge estimation of Li-ion batteries," *IEEE Transactions on Industrial Electronics*, vol. 65, no. 8, pp. 6730-6739, 2017.
[34] F. Yang, S. Zhang, W. Li, and Q. Miao, "State-of-charge estimation of lithium-ion batteries using LSTM and UKF," *Energy*, vol. 201, p. 117664, 2020/06/15/ 2020, doi: https://doi.org/10.1016/j.energy.2020.117664.
[35] W. He, N. Williard, C. Chen, and M. Pecht, "State of charge estimation for Li-ion batteries using neural network modeling and unscented Kalman filter-based error cancellation," *International Journal of Electrical Power & Energy Systems*, vol. 62, pp. 783-791, 2014.
[36] D. E. Rumelhart, G. E. Hinton, and R. J. Williams, "Learning representations by back-propagating errors," *nature*, vol. 323, no. 6088, pp. 533-536, 1986.
[37] C. Li, F. Xiao, and Y. Fan, "An approach to state of charge estimation of lithium-ion batteries based on recurrent neural networks with gated recurrent unit," *Energies*, vol. 12, no. 9, p. 1592, 2019.
[38] A. Beke and T. Kumbasar, "Learning with type-2 fuzzy activation functions to improve the performance of deep neural networks," *Engineering Applications of Artificial Intelligence*, vol. 85, pp. 372-384, 2019.
[39] J. Pomerat, A. Segev, and R. Datta, "On Neural Network Activation Functions and Optimizers in Relation to Polynomial Regression," in *2019 IEEE International Conference on Big Data (Big Data)*, 2019: IEEE, pp. 6183-6185.
[40] A. Lydia and S. Francis, "Adagrad—An optimizer for stochastic gradient descent," *Int. J. Inf. Comput. Sci.*, vol. 6, no. 5, 2019.
[41] C. Bian, H. He, and S. Yang, "Stacked bidirectional long short-term memory networks for state-of-charge estimation of lithium-ion batteries," *Energy*, vol. 191, p. 116538, 2020.
[42] A. Poernomo and D.-K. Kang, "Biased dropout and crossmap dropout: learning towards effective dropout regularization in convolutional neural network," *Neural Networks*, vol. 104, pp. 60-67, 2018.
[43] N. Srivastava, G. Hinton, A. Krizhevsky, I. Sutskever, and R. Salakhutdinov, "Dropout: a simple way to prevent neural networks from overfitting," *The journal of machine learning research*, vol. 15, no. 1, pp. 1929-1958, 2014.
[44] B. Chen, X. Liu, H. Zhao, and J. C. Principe, "Maximum correntropy Kalman filter," *Automatica*, vol. 76, pp. 70-77, 2017.
[45] Z. Chen, J. Zhou, F. Zhou, and S. Xu, "State-of-charge estimation of lithium-ion batteries based on improved H infinity filter algorithm and its novel equalization method," *Journal of Cleaner Production*, p. 125180, 2020/11/18/ 2020, doi: https://doi.org/10.1016/j.jclepro.2020.125180.
[46] X. Shu, G. Li, Y. Zhang, J. Shen, Z. Chen, and Y. Liu, "Online diagnosis of state of health for lithium-ion batteries based on short-term charging profiles," *Journal of Power Sources*, vol. 471, p. 228478, 2020/09/30/ 2020, doi: https://doi.org/10.1016/j.jpowsour.2020.228478.

[47] X. Hu, F. Feng, K. Liu, L. Zhang, J. Xie, and B. Liu, "State estimation for advanced battery management: Key challenges and future trends," *Renewable and Sustainable Energy Reviews*, vol. 114, p. 109334, 2019/10/01/ 2019, doi: https://doi.org/10.1016/j.rser.2019.109334.
[48] G. Hunt, "USABC electric vehicle battery test procedures manual," *Washington, DC, USA: United States Department of Energy*, 1996.
[49] F. Yang, W. Li, C. Li, and Q. Miao, "State-of-charge estimation of lithium-ion batteries based on gated recurrent neural network," *Energy*, vol. 175, pp. 66-75, 2019/05/15/ 2019, doi: https://doi.org/10.1016/j.energy.2019.03.059.
[50] J. Hong, Z. Wang, W. Chen, L.-Y. Wang, and C. Qu, "Online joint-prediction of multi-forward-step battery SOC using LSTM neural networks and multiple linear regression for real-world electric vehicles," *Journal of Energy Storage*, vol. 30, p. 101459, 2020.